Nuclear Quantum Effects Affect Bond Orientation of Water at the Water-Vapor Interface

Yuki Nagata, Ruben E. Pool, Ellen H. G. Backus, and Mischa Bonn

Max-Planck Institute for Polymer Research Ackermannweg 10, 55128 Mainz, Germany

(Received 30 July 2012; revised manuscript received 4 October 2012; published 29 November 2012)

Using combined theoretical and experimental approaches, we demonstrate that the bond orientation of water at the water-vapor interface depends markedly on the water isotope (H-D) composition. While the interfacial water structures of H_2O and D_2O are indistinguishable, the intramolecular symmetry breaking in HDO is directly reflected at the surface: the OD bonds preferably orient down towards the bulk water, whereas the OH bond tends to orient up into the vapor phase. Path integral molecular dynamics simulations show good agreement with surface-specific sum-frequency generation (SFG) spectroscopy results, revealing that the distinct interfacial bond orientations originate from nuclear quantum effects. The enhanced localization of the heavier D atom leads to stronger hydrogen bonds, giving rise to OD bonds pointing down into the bulk.

DOI: 10.1103/PhysRevLett.109.226101 PACS numbers: 68.03.Hj, 31.15.xk, 36.20.Ng, 78.20.Bh

Water in condensed phases is unique in its strong, anisotropic intermolecular interactions. These interactions occur through hydrogen bonds (HBs) between a H atom on one molecule and an O atom of another, and collectively lead to a structurally rich network. Nuclear quantum effects cause a non-negligible zero point energy (ZPE) for low mass nuclei, specifically for H atoms. The high density of H atoms in water makes nuclear quantum effects significant [1–5]. These effects show up when H atoms are replaced by heavier D atoms, giving rise to different macroscopic properties of H_2O and D_2O in a nonintuitive fashion: D_2O melts at a temperature 3.8 K higher than H_2O, the temperature of the maximum density increased by 7.2 K in D_2O compared with H_2O, protein stability is increased in D_2O [4], D_2O ice is expanded relative to H_2O [5]. Isotopic substitution of water has provided an indispensable tool for studying nuclear quantum effects on water properties, structure, and dynamics.

While significant understanding has been reached regarding the different HB interactions due to the isotope effects in bulk water [1–6], these effects have not been fully examined at aqueous interfaces. Aqueous interfaces require the interruption of the HB network, exhibiting specific anisotropic properties. At the water-vapor interface, this results in some interfacial water molecules having "free" non-H-bonded OH groups sticking into the vapor phase. The water-vapor interface is of intrinsic interest owing to its ubiquity in nature, and also serves as a paradigmatic model system for extended hydrophobic surfaces. In addition to these fundamental interests, nuclear quantum effects at aqueous interfaces are relevant for interface-specific vibrational spectroscopy studies such as sum-frequency generation (SFG), where isotopic dilution has been routinely used to avoid intra- and intermolecular couplings of interfacial water [7–12]. Knowledge of the isotope effect is essential to verify the implicit assumption that interfacial water structures for the mixture of H_2O, D_2O, and HDO are identical.

In this Letter, we explore the nuclear quantum effects on the water structure near the vapor interface. We perform path integral molecular dynamics (PIMD) simulations to include the nuclear quantum effects explicitly [13]. Our simulation shows that the broken symmetry of the HB interactions in HDO gives rise to distinct OH and OD bond orientations at the vapor interface. We confirm distinct bond orientations by measuring SFG spectra experimentally and comparing them with the PIMD simulations.

PIMD simulations were performed with 80 water molecules by using the CP2K package program. To simplify the discussion, we used pure H_2O, D_2O, and HDO instead of their mixture. The simulation cell was set to 13.2 Å for the x and y axes and 70 Å for the z axis, where the xy plane was parallel to the interface and the z axis was parallel to the surface normal. Periodic boundary conditions were used. We employed the q-SPC/Fw water model [6]. The Coulomb summation was done with the smooth particle mesh Ewald method with $14 \times 14 \times 70$ grids. First, we ran classical MD simulations to sample 30 configurations for the HDO-vapor interface at 285, 300, and 315 K and 15 configurations for the H_2O vapor and D_2O vapor interfaces at 300 K. The system temperature was controlled by the Nose-Hoover thermostat. Then, the PIMD simulations with the colored noise thermostat based on generalized Langevin equations (GLE) [14] were performed at each temperature, where the independent Gaussian number $N_s + 1 = 5$, the minimum frequency of thermostating $\omega_{\mathrm{min}} = 1\ \mathrm{cm}^{-1}$, and the maximum frequency $\omega_{\mathrm{max}} = 10000\ \mathrm{cm}^{-1}$. The parameters for the GLE thermostat were obtained from Ref. [15]. The number of beads for the PIMD simulation, P, was set to 24. $P \geq 24$ is sufficient for reproducing the quantum distribution function and energy reasonably [6]. The time step was set to 0.1 fs. 100 ps PIMD runs were conducted to equilibrate the systems. Sequentially, we ran over 200 ps PIMD simulations to sample water configurations, which were used for

calculating the bond orientations, the HB number, and the SFG spectra.

The possible anisotropy of water at interfaces can be characterized by the OH (OD) bond orientation [16], which is readily qualified by the axial profile of the angle θ between the OH (OD) bond and the surface normal. Note that two angles θ for each H_2O (D_2O) molecule were calculated. The origin point of the z coordinate was set to the center of mass for the system. The Gibbs dividing surface is located at $|z| = 6.8$ Å. (see Supplemental Material [17]) Figure 1 depicts the averaged angle $\langle\cos\theta\rangle$ for H_2O, D_2O, and HDO. The H_2O and D_2O curves overlap, indicating that the OH bond orientation of H_2O is similar to the OD orientation of D_2O. On average both the OH and OD bonds orient to the vapor phase for $|z| > 6.7$ Å and orient to the bulk for 3.0 Å $< |z| < 6.7$ Å, while specific orientation vanishes for $|z| < 3.0$ Å. While H_2O and D_2O give indiscernible results, the OH bond orientation of HDO is markedly different from the OD bond. In the bulk region ($|z| < 2.0$ Å), the OH and OD bonds show no specific orientations. Approaching the interface, the OH bond shows slightly stronger orientation toward the bulk than the OD bond for 2.0 Å $< |z| < 4.2$ Å, while the opposite tendency can be found for 4.2 Å $< |z| < 6.1$ Å. In 6.1 Å $< |z| < 7.4$ Å, the OH and OD bonds orient to the vapor and the bulk, respectively. Both the OH and OD bonds orient to the vapor region in $|z| > 7.4$ Å, but $\cos\theta$ is larger for the OH bond than the OD bond. This distinct orientation arises from nuclear quantum effects, as evidenced by its disappearance as reducing the number of beads for the PIMD simulation, P, and by its temperature dependence. At 285 K the distinct OH and OD bond orientations were enhanced while they decreased at 315 K (see Supplemental Material [17]), which is consistent with the enhanced nuclear quantum effect at lower temperature. The symmetry is broken due to the nuclear quantum effects, so that the OH and OD bonds tend to orient toward the vapor and the bulk regions, respectively.

To elucidate the intermolecular interactions underlying the asymmetric bond orientation of HDO, we calculated the numbers of O-H $\cdots$ O and O-D $\cdots$ O HBs. The presence of the HB was defined as 1.59 Å $< r_{H\cdots O} < 2.27$ Å and $\alpha < 40°$, where $r_{H\cdots O}$ denotes the intermolecular OH (OD) distance and α the angle between intra- and intermolecular OH (OD) bonds (see the sketch in the left side of Fig. 2) [18]. Figure 2 displays the axial profiles of the HB numbers for O-H $\cdots$ O$\langle n_H\rangle$ and for O-D $\cdots$ O$\langle n_D\rangle$. In the bulk region ($|z| < 2.0$ Å), $\langle n_D\rangle$ is 2% larger than $\langle n_H\rangle$, which is consistent with a more diffusive O-H $\cdots$ O angle compared to the O-D $\cdots$ O angle in bulk water [3]. Moving from the bulk to the vapor region, the difference between $\langle n_D\rangle$ and $\langle n_H\rangle$ increases, indicating that increased O-D $\cdots$ O HBs stabilizes the interfacial water structure at the cost of the concomitant entropy decrease. More O-D $\cdots$ O HBs than O-H $\cdots$ O HBs make the enrichment of the free OH bonds pointing toward the vapor phase. Our finding can be connected with the previous study of isotopic fractionation of H_2O-HDO water [19]. By decomposing the kinetic energy into the components arising from the OH bond vector and two vectors orthogonal to the OH bond, Markland and Berne have showed that the components arising from the vectors orthogonal to the OH bond stabilizes the D excess in liquid compared to gas. This indicates that the free OH bond and hydrogen-bonded OD bond is favored compared with the free OD bond and hydrogen-bonded OH bond. This is consistent with our

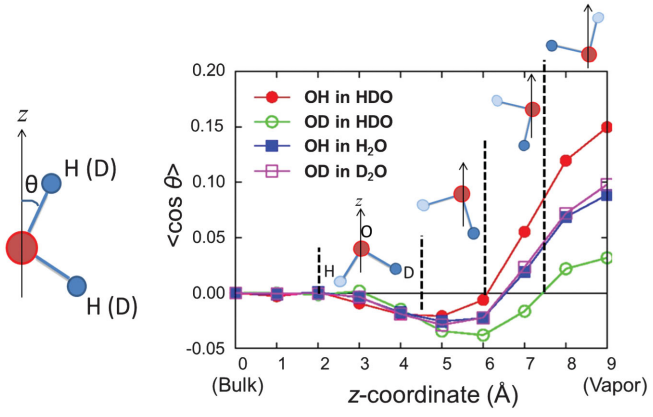

FIG. 1 (color). (Left) Pictorial representation of the angle θ between the OH (OD) bond and the surface normal. (Right) Axial distribution of average angles $\langle\cos\theta\rangle$. Lines are guides for the eyes. The water molecules illustrate the average orientations of HDO (D dark blue, H light blue) in the different regions. The positive and negative z-axis points up to the vapor region and to the bulk water region, respectively. Red filled circle, green open circle, blue filled square, and purple open square denote the OH group in HDO, the OD group in HDO, the OH group in H_2O, and the OD group in D_2O, respectively.

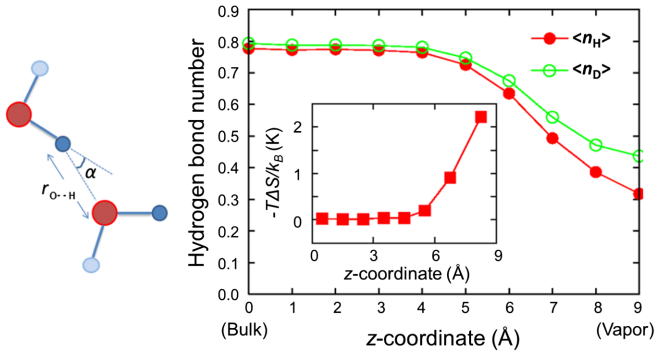

FIG. 2 (color online). (Left) Pictorial representation of the distance $r_{H\cdots O}$ and the angle α for the HB definition. (Right) Depth profiles of the HB numbers for the O-H $\cdots$ O$\langle n_H\rangle$ and O-D $\cdots$ O$\langle n_D\rangle$ at the HDO-vapor interface. The free energy loss $-T\Delta S/k_b$ originated from the entropy decrease due to the distinct OH and OD bond orientations are plotted in the inset. The lines are a guide for the eyes.

observation. This stronger H bond of a D atom arises from the libration mode [20,21].

The entropic cost of creating this asymmetry should be balanced by the O-H$\cdots$O and O-D$\cdots$O HB energy difference. This HB energy difference results in a melting point difference of 3.8 K between bulk H_2O and D_2O. In the following we will demonstrate that an energy difference corresponding to a few K originating from the nuclear quantum effects is enough to generate the distinct OH and OD bond orientations at the HDO-vapor interface. Our calculation methodology is as follows: The entropy would be maximal when the OH and OD bond orientations are the same. The entropy for this hypothetical case is denoted by S_1. On the other hand, our PIMD simulations show different preferred orientations of the OH and OD bonds. The entropy of this case is called S_2. The entropy decrease due to the distinct bond orientations can then be calculated as $\Delta S = S_2\text{-}S_1$. S_1 and S_2 were calculated from the histograms of the OH and OD bond orientations (see Supplemental Material [17]). The axial profile of $-T\Delta S/k_B$ for one HDO molecule is plotted in the inset of Fig. 2, indicating that $-T\Delta S/k_B$ increases with approaching the vapor region and reaches a maximum value of a few K, i.e., the same magnitude as the melting point difference between H_2O and D_2O. This shows that energetic gain and entropic costs for the preferred bond orientations are balanced.

Our PIMD simulations predict that more free OH bonds than free OD bonds are present at the isotopically diluted water-vapor interface due to nuclear quantum effects. We used vibrational SFG spectroscopy to establish this enrichment of free OH bonds experimentally. As SFG is a second-order process, it is forbidden in bulk media and therefore provides an excellent tool to probe the surface composition [22]. In our study, SFG spectra at the water-vapor interface were recorded for a range of different isotopic dilutions, two of which are plotted in Figs. 3(a) and 3(b), under ssp polarization (SFG and visible s polarized, infrared p polarized). The free OH (OD) stretch vibration shows up in the SFG spectra of the water-vapor interface as a narrow resonant peak at $\sim$3700 cm^{-1} ($\sim$ 2750 cm^{-1}) [7–11,22]. To probe the OH bond enrichment at the vapor interface, the SFG spectra for the OH and OD stretch regions were measured as a function of isotopic dilution. To decompose the SFG intensity to the free OH (OD), hydrogen-bonded OH (OD), and nonresonant contributions, we fit the SFG intensities by using

$$I_{ssp}(\omega) \propto |\chi^{(2)}_{ssp}(\omega)|^2 = \left| A_{NR}e^{i\varphi_{NR}} + \sum_i^n \frac{A_i}{\omega - \omega_i + i\Gamma_i} \right|^2, \quad (1)$$

where A_{NR} is the nonresonant amplitude, φ_{NR} the nonresonant phase, and A_i, ω_i, and Γ_i the peak intensity, center frequency, and width of the ith Lorentzian, respectively. Details of the fitting procedure can be found in the Supplemental Material [17]. The fitted curves in Figs. 3(a) and 3(b) accurately reproduce the SFG spectral shapes. Im$[\chi^{(2)}_{ssp}(\omega)]$ constructed from these fitting parameters is shown in Figs. 3(c) and 3(d). Since Im$[\chi^{(2)}_{ssp}(\omega)]$ is directly related to the spectral shape of the resonances, we used it to calculate the free OH [OD] peak area $A_{OH}(x)$ [$A_{OD}(x)$] for the concentration x of H_2O [D_2O], which was

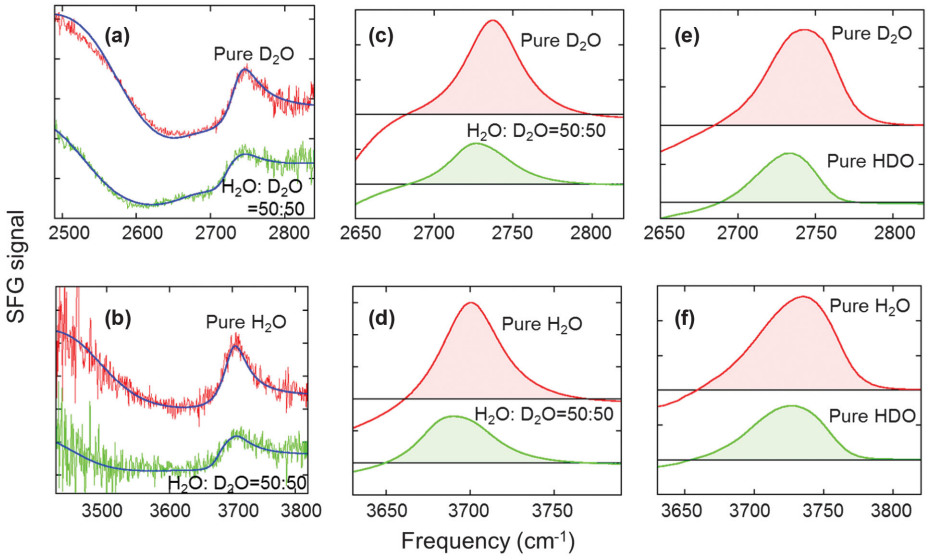

FIG. 3 (color). (a, b) Experimentally measured SFG spectra $|\chi^{(2)}_{ssp}(\omega)|^2$ (red and green) and their fitted curves (blue), (c), (d) Im$[\chi^{(2)}_{ssp}(\omega)]$ constituted by the fitted parameters, and (e), (f) simulated Im$[\chi^{(2)}_{ssp}(\omega)]$. Top panels (a),(c),(e) and down panels (b), (d), (f) display the spectra in the OD and OH stretching regions, respectively. Filled areas in (c), (d), (e), and (f) represent the free OH or OD bond peak areas (see main text).

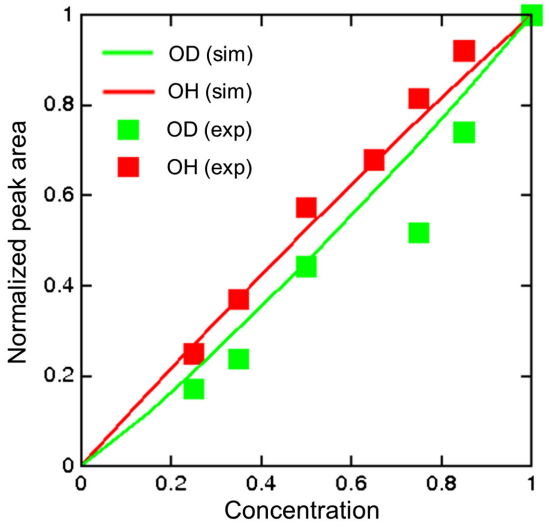

FIG. 4 (color online). Normalized free OH and OD bond peak areas $A(x)/A(x = 1.0)$ as a function of the concentration x from the SFG experiments (squares) and the PIMD simulations (lines).

defined as the peak area of the fitted $\mathrm{Im}[\chi^{(2)}_{ssp}(\omega)]$ above a baseline defined for the OH [OD] stretch region at 3770[2800] cm^{-1}. Subsequently, in order to enable direct comparison between the SFG experiments and the PIMD simulations, we simulated $\mathrm{Im}[\chi^{(2)}_{ssp}(\omega)]$ by using the PIMD snapshots and calculated the normalized peak areas. The simulation details are written in the Supplemental Material [17]. The simulated SFG spectra of H_2O, D_2O, and HDO are shown in Figs. 3(e) and 3(f). Since diluted water consists of a mixture of H_2O, D_2O, and HDO, $\mathrm{Im}[\chi^{(2)}_{ssp}(\omega)]$ for the mixtures can be calculated by

$$\chi^{(2)}(\omega) = [\mathrm{H_2O}]\chi^{(2)}_{\mathrm{H_2O}}(\omega) + [\mathrm{HDO}]\chi^{(2)}_{\mathrm{HDO}}(\omega) + [\mathrm{D_2O}]\chi^{(2)}_{\mathrm{D_2O}}(\omega), \quad (2)$$

where $[H_2O]$, $[D_2O]$, and [HDO] are the concentrations of H_2O, D_2O, and HDO, respectively. By utilizing the equilibrium constant $K = [\mathrm{HDO}]^2/[\mathrm{H_2O}][\mathrm{D_2O}]$ of 3.86 [23], we calculated $\mathrm{Im}[\chi^{(2)}_{ssp}(\omega)]$ for different H_2O/D_2O concentrations. As with the experimental data, the normalized free OH [OD] bond peak areas, $A_{\mathrm{OH}}(x)$ [$A_{\mathrm{OD}}(x)$], were calculated by integrating the peak areas above the baseline $\mathrm{Im}[\chi^{(2)}_{ssp}(\omega)] = 0$.

In Fig. 4, the experimentally obtained normalized bond areas for the different isotopic dilutions, $A_{\mathrm{OH}}(x)/A_{\mathrm{OH}}(x = 1.0)$ and $A_{\mathrm{OD}}(x)/A_{\mathrm{OD}}(x = 1.0)$, are plotted as squares while the simulated peak areas are represented by solid lines. Good agreement can be seen between the simulated normalized peak areas and the experimentally measured data with exceptions at the high concentration of the OD stretch mode. For high D_2O concentration, the free D_2O shoulder peak at $\sim$2665 cm^{-1} contributes to the signal, complicating the estimation of the free OD bond peak areas. Nevertheless, both the SFG spectra and the PIMD simulations indicate that the normalized free OH peak areas consistently lie above the normalized free OD peak areas. Since without distinct bond orientations SFG signals for both the free OH and OD stretches would be reduced with the concentration in the same way [8,10], this result confirms that more free OH bonds than free OD bonds are present at the vapor interface in isotopic mixtures. Note that we assumed that the concentration of the H_2O, D_2O, and HDO is in the same manner with the bulk water in this study. We will address the isotope effect of the distribution of water species in the mixture of H_2O, D_2O, and HDO.

In summary, we have simulated the H_2O, D_2O, and HDO-vapor interfaces by using the PIMD simulations to incorporate the nuclear quantum effects explicitly. The OH bond orientation at the H_2O-vapor interface was similar to the OD bond orientation at the D_2O-vapor interfaces. In contrast, our PIMD simulations indicate that the OH and OD bonds have distinct orientation at the HDO-vapor interface; the OD bond tends to orient toward the bulk region, while the OH bond tends to orient toward the vapor region. This distinct OH and OD bond orientations have been identified by experimentally observed SFG spectra and the simulated SFG spectra from the PIMD simulations. The current study confirms that nuclear quantum effects generate distinct OH and OD bond orientations at the water-vapor interface and indicates that nuclear quantum effects are non-negligible for quantitative analyses in interface-specific studies, e.g., SFG at isotopic diluted samples.

Y. N. and R. E. P. have contributed equally to this work.

[1] Y. S. Badyal, D. L. Price, M.-L. Saboungi, D. R. Haeffner, and S. D. Shastri, J. Chem. Phys. **116**, 10833 (2002).
[2] H. A. Stern and B. J. Berne, J. Chem. Phys. **115**, 7622 (2001).
[3] B. Chen, I. Ivanov, M. L. Klein, and M. Parrinello, Phys. Rev. Lett. **91**, 215503 (2003); J. A. Morrone and R. Car, Phys. Rev. Lett. **101**, 017801 (2008).
[4] Y. M. Efimova, S. Haemers, B. Wierczinski, W. Norde, and A. A. van Well, Biopolymers **85**, 264 (2007); Y. Cho, L. B. Sagle, S. Iimura, Y. Zhang, H. Kherb, A. Chilkoti, J. M. Scholtz, and P. S. Cremer, J. Am. Chem. Soc. **131**, 15 188 (2009).
[5] B. Pamuk, J. M. Soler, R. Ramirez, C. P. Herrero, P. W. Stephens, P. B. Allen, and M.-V. Fernandez-Serra, Phys. Rev. Lett. **108**, 193003 (2012).
[6] F. Paesani, W. Zhang, D. A. Case, T. E. Cheatham, III, and G. A. Voth, J. Chem. Phys. **125**, 184507 (2006); F. Paesani and G. A. Voth, J. Phys. Chem. B **113**, 5702 (2009).
[7] E. A. Raymond, T. L. Tarbuck, and G. L. Richmond, J. Phys. Chem. B **106**, 2817 (2002); E. A. Raymond, T. L. Tarbuck, M. G. Brown, G. L. Richmond, J. Phys. Chem. B **107**, 546 (2003).

[8] C. S. Tian and Y. R. Shen, J. Am. Chem. Soc. **131**, 2790 (2009).
[9] P. A. Pieniazek, C. J. Tainter, and J. L. Skinner, J. Am. Chem. Soc. **133**, 10 360 (2011).
[10] S. Nihonyanagi, T. Ishiyama, T.-K. Lee, S. Yamaguchi, M. Bonn, A. Morita, and T. Tahara, J. Am. Chem. Soc. **133**, 16 875 (2011).
[11] I. V. Stiopkin, C. Weeraman, P. A. Pieniazek, F. Y. Shalhout, J. L. Skinner, and A. V. Benderskii, Nature (London) **474**, 192 (2011).
[12] M. Sovago, R. K. Campen, G. W. H. Wurpel, M. Müller, H. J. Bakker, and M. Bonn, Phys. Rev. Lett. **100**, 173901 (2008).
[13] D. Chandler and P. G. Wolynes, J. Chem. Phys. **74**, 4078 (1981).
[14] M. Ceriotti, M. Parrinello, T. E. Markland, and D. E. Monolopoulos, J. Chem. Phys. **133**, 124104 (2010).
[15] http://gle4md.berlios.de/.
[16] T. Ishiyama and A. Morita, J. Phys. Chem. C **111**, 721 (2007).
[17] See Supplemental Material at http://link.aps.org/supplemental/10.1103/PhysRevLett.109.226101 for the simulation methodology to calculate the SFG signal, the details of the experimental SFG setup and further simulation, and experimental data.
[18] I.-F. W. Kuo and C. J. Mundy, Science **303**, 658 (2004).
[19] T. E. Markland and B. J. Berne, Proc. Natl. Acad. Sci. U.S.A. **109**, 7988 (2012).
[20] A. K. Soper and C. J. Benmore, Phys. Rev. Lett. **101**, 065502 (2008).
[21] U. Bergmann, D. Nordlund, Ph. Wernet, M. Odelius, L. G. M. Pettersson, and A. Nilsson, Phys. Rev. B **76**, 024202 (2007).
[22] Q. Du, R. Superfine, E. Freysz, and Y. R. Shen, Phys. Rev. Lett. **70**, 2313 (1993).
[23] F. O. Libnau, A. A. Christy, and O. M. Kvalheim, Appl. Spectrosc. **49**, 1431 (1995).